Supplement of Atmos. Meas. Tech., 18, 2425–2437, 2025
https://doi.org/10.5194/amt-18-2425-2025-supplement

Atmospheric Measurement Techniques
Open Access
EGU

Supplement of

A solid-state infrared laser for two-step desorption–ionization processes in single-particle mass spectrometry

Marco Schmidt et al.

Correspondence to: Johannes Passig (johannes.passig@uni-rostock.de)

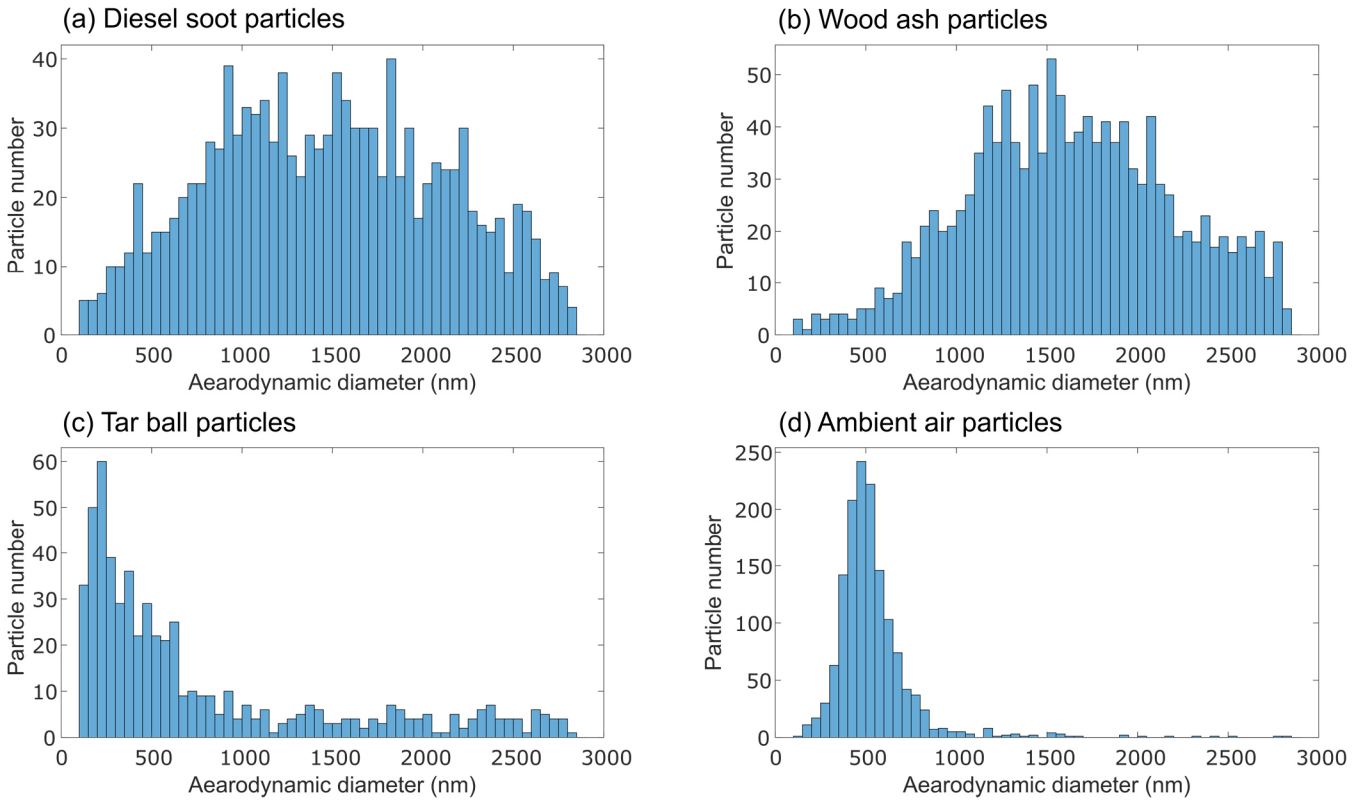

Figure S1 Particle size distributions, n = 1200 each, of the laboratory and ambient air particles measured using the optical sizing unit of the SPMS: **(a)** Diesel soot particles; **(b)** Wood ash particles; **(c)** Tar ball particles; and **(d)** Ambient air particles.

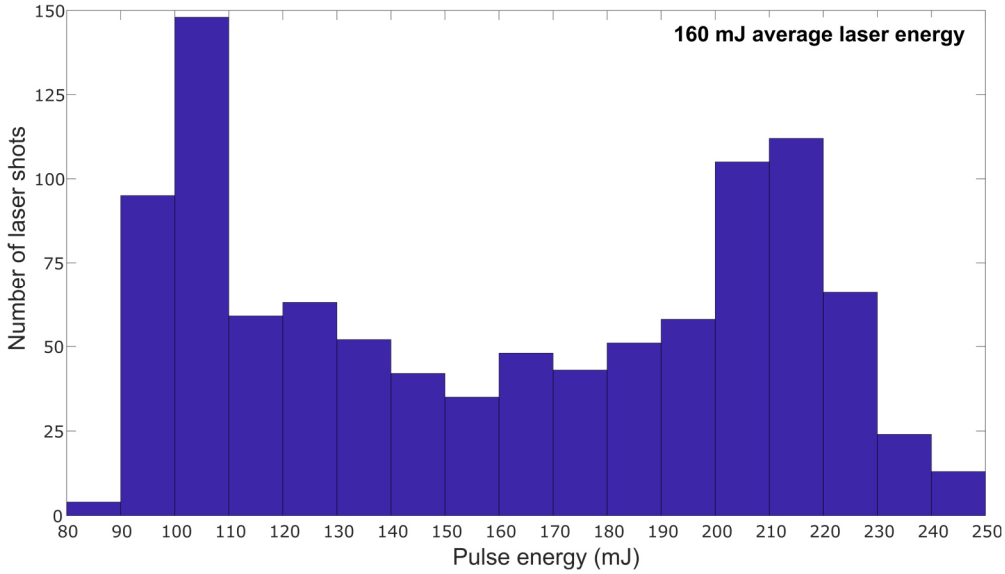

Figure S2 Pulse energies of 1022 laser pulses from the Er:YAG laser. The observed high fluctuation is attributed to the random nature of particle events inducing thermal lensing effects in the laser resonator; the average pulse energy was determined to be 160 mJ.

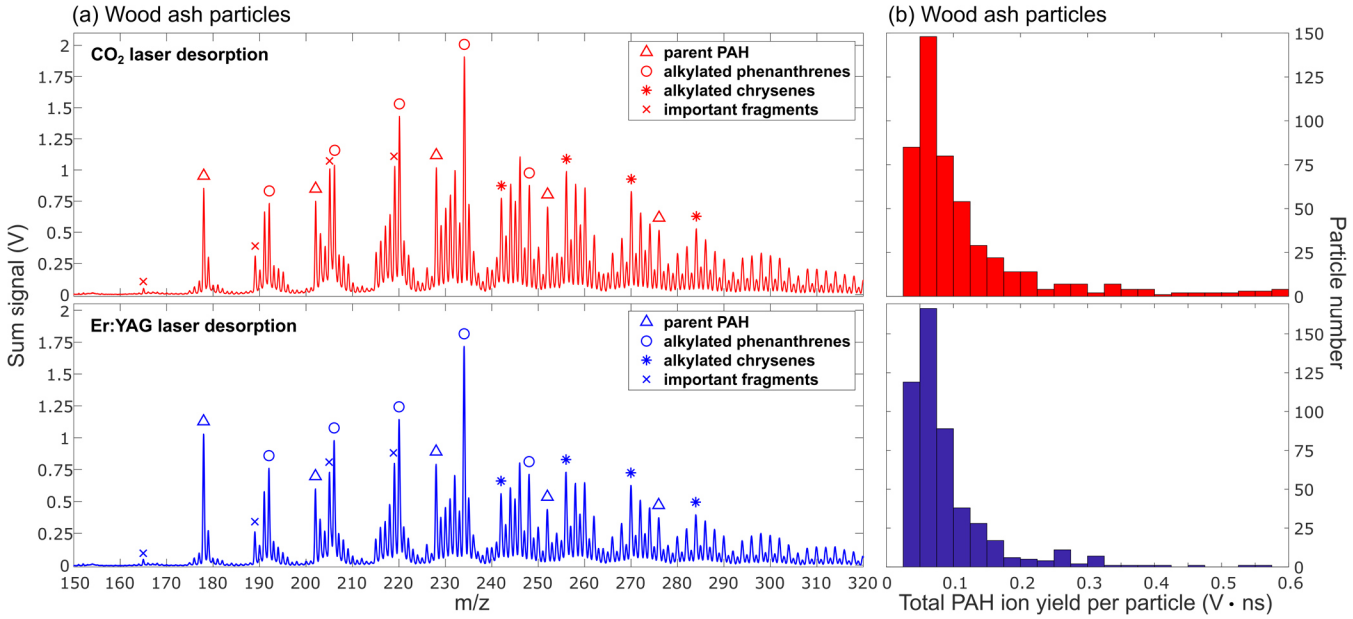

Figure S3 (a) Wood ash particles (n = 500 each) exhibit a very different PAH profile in the LD-REMPI ionization than diesel soot particles, and they show the softwood combustion marker retene (m/z = 234), a thermal degradation product of resin acids. There are also some signals from higher-mass molecules, possibly from oxidized PAHs and other combustion products with aromatic rings, which can be ionized in the LD-REMPI scheme. However, in direct comparison, there are almost no differences between the CO_2 laser and the Er:YAG laser for LD. **(b)** The single-particle signal intensity of PAHs again shows a few more particles with strong PAH signals for the CO_2 laser. The hit rate for PAHs was low, with only 2 % (4 %) of the optically detected particles showing a PAH spectrum when the CO_2 laser (Er:YAG laser) was used due to the nature of the sample, which contains many burnt ash particles and fewer OC/soot particles containing PAHs (Dall'Osto et al., 2016; Healy et al., 2015).

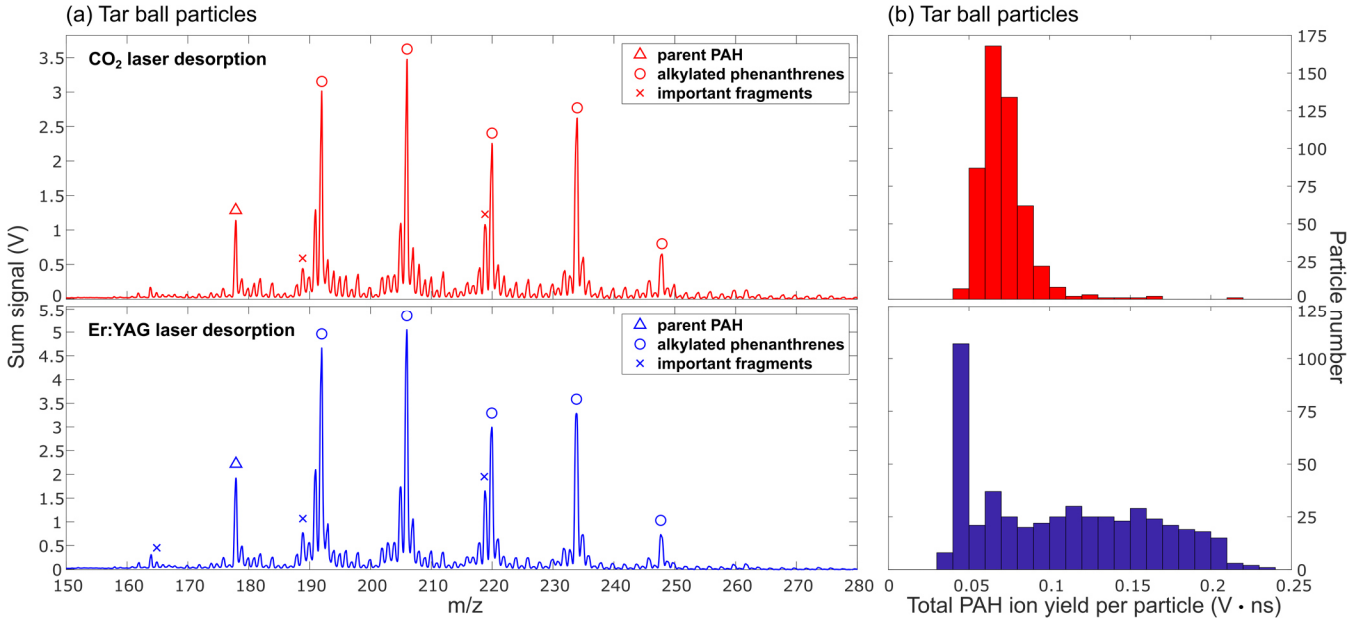

Figure S4 In our case of sprayed wood tar as a proxy for organic aerosols from wood combustion, the sum PAH spectra (n = 500 each) show almost exclusively alkylated phenanthrenes, in contrast to a more sophisticated tar ball model that we analyzed in a previous study using the

same LD-REMPI technique (Li et al., 2019). However, they appear to be an appropriate and easier to generate model to study LD for the highly relevant organic aerosols from wood combustion, as they have comparable physical properties such as high viscosity, low volatility, and a brown color with high absorption in the UV-VIS due to their PAH content (Jacobson, 2012; Brege et al., 2021; Li et al., 2019). While there are no qualitative differences in the mass spectra between the two lasers used for LD, the Er:YAG laser produced intense PAH spectra more often for this particle type. This can be explained by the strong absorption of the solvent methanol at the 3 µm wavelength of the Er:YAG laser. In addition, it was difficult to determine the hit rate in these experiments, because there was a small background of the PAH signature from particle evaporation effects in the inlet, even when no particle was hit. A particle hit was defined when the sum of the peak areas exceeded 30 mV · ns, based on the distribution of signal intensities per laser shot. This results in a hit rate of 54 % (49 %) for the CO_2 laser (Er:YAG laser).

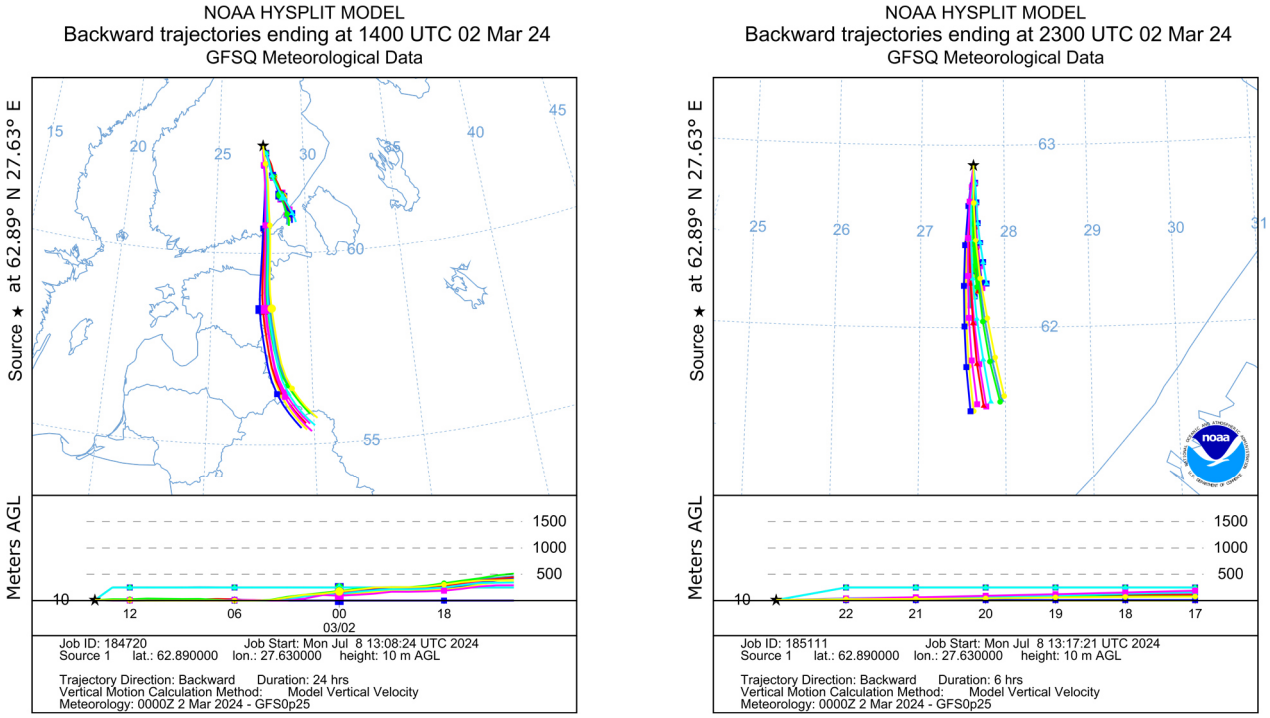

Figure S5 HYSPLIT backward trajectories for 24 h run time (left) for the ambient air experiments with the LD-REMPI approach and with 6 h run time for the subsequent experiments with the combined LD-REMPI/LDI approach (right), both ending at the measurement location.

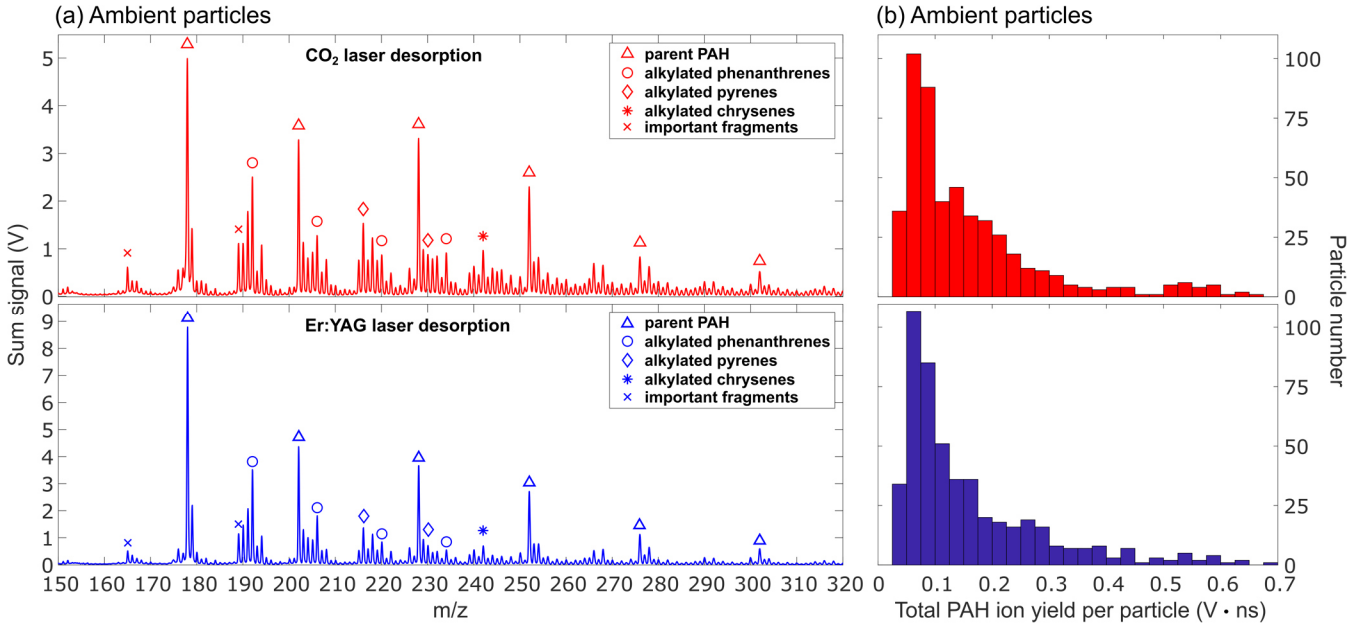

Figure S6 (a) Sum PAH mass spectra from ambient air particles (n = 500 each) measured in the LD-REMPI ionization approach. In direct comparison, the mass spectral signatures are similar between the CO_2 laser and the Er:YAG laser for LD. The Er:YAG produces slightly higher signal intensities for parent PAH, especially for m/z = 178, as discussed in Section 3.3. **(b)** The single-particle signal intensities of PAHs are also comparable for both lasers.

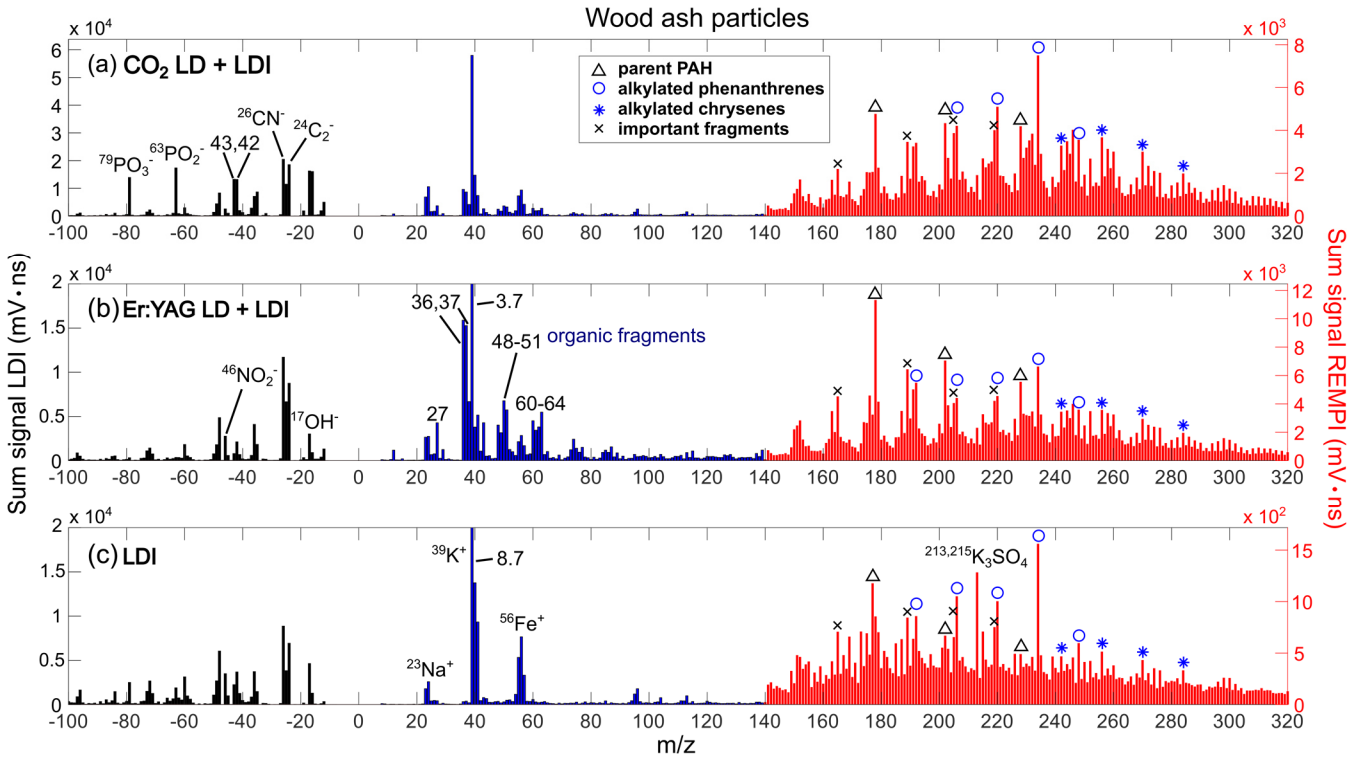

Figure S7 For wood ash particles, the combined method yields comparable results for **(a)** the CO_2 laser and **(b)** the Er:YAG laser applied for LD. Due to the nature of these particles, the single-step LDI method also produces clear PAH signatures, but with a lower sensitivity (compare the Y-axes on the right), n = 500 each.

(a) Cluster analysis of LD/LDI mass spectra with CO_2 laser

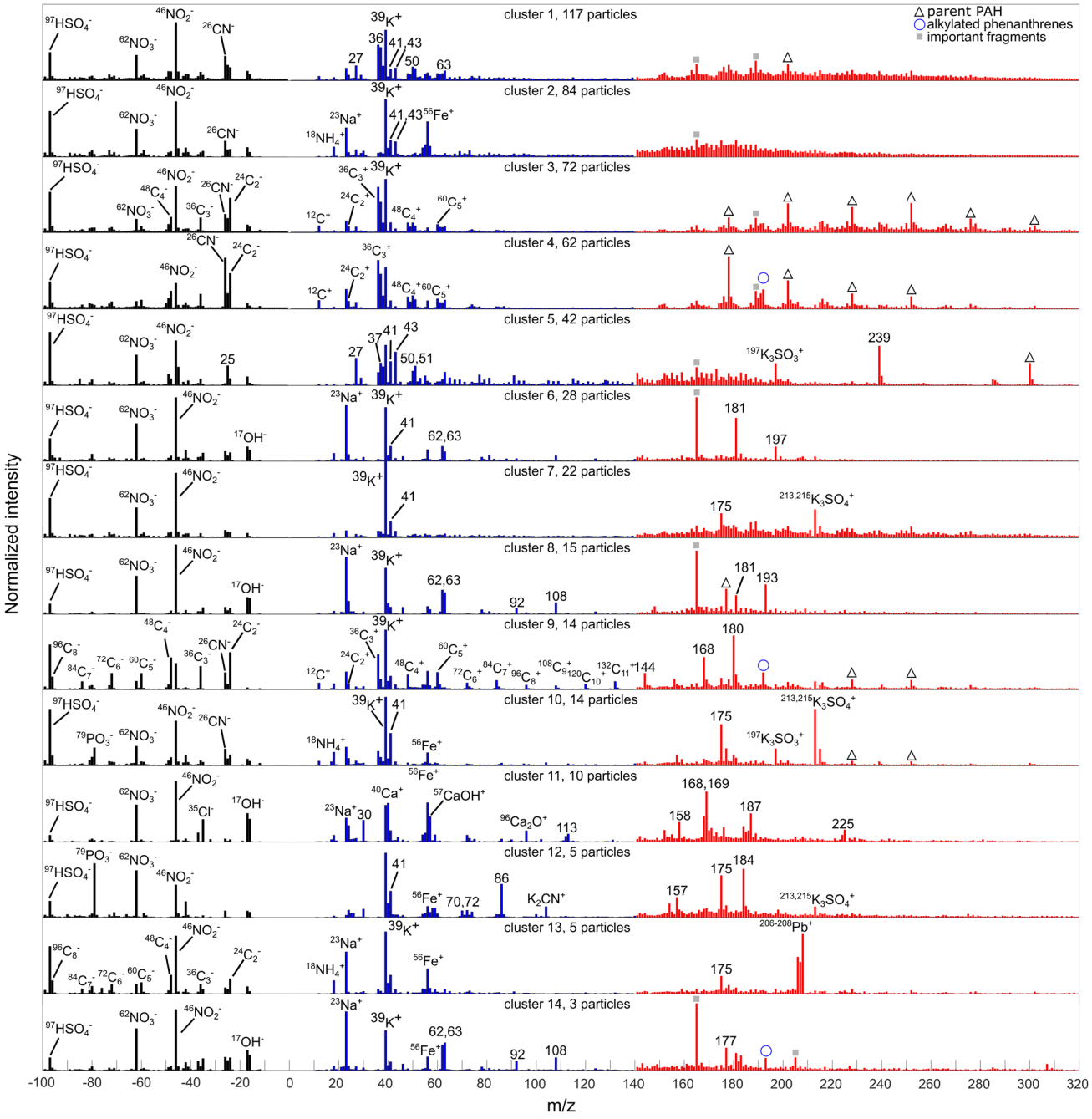

(b) Cluster analysis of LD/LDI mass spectra with Er:YAG laser

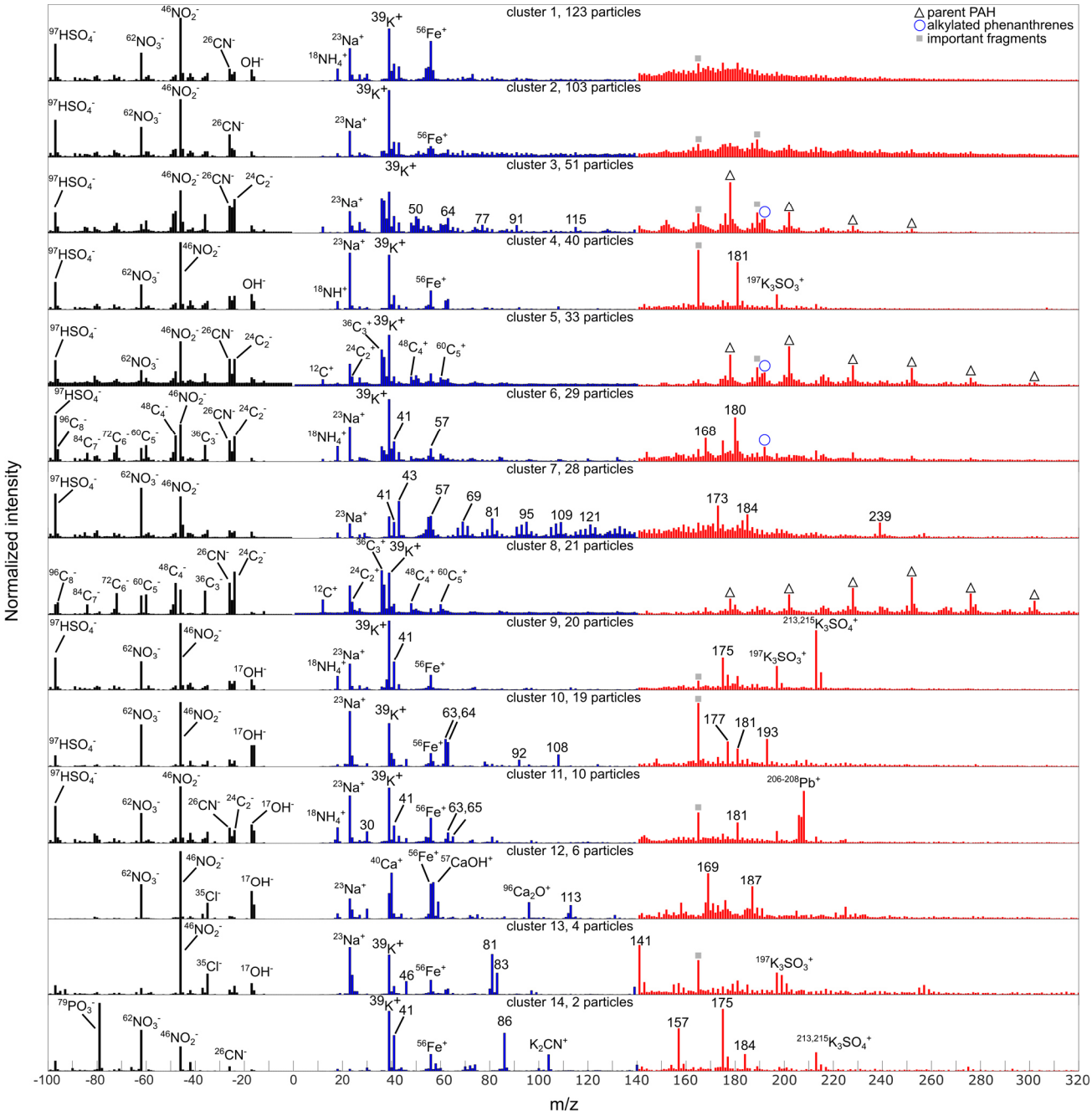

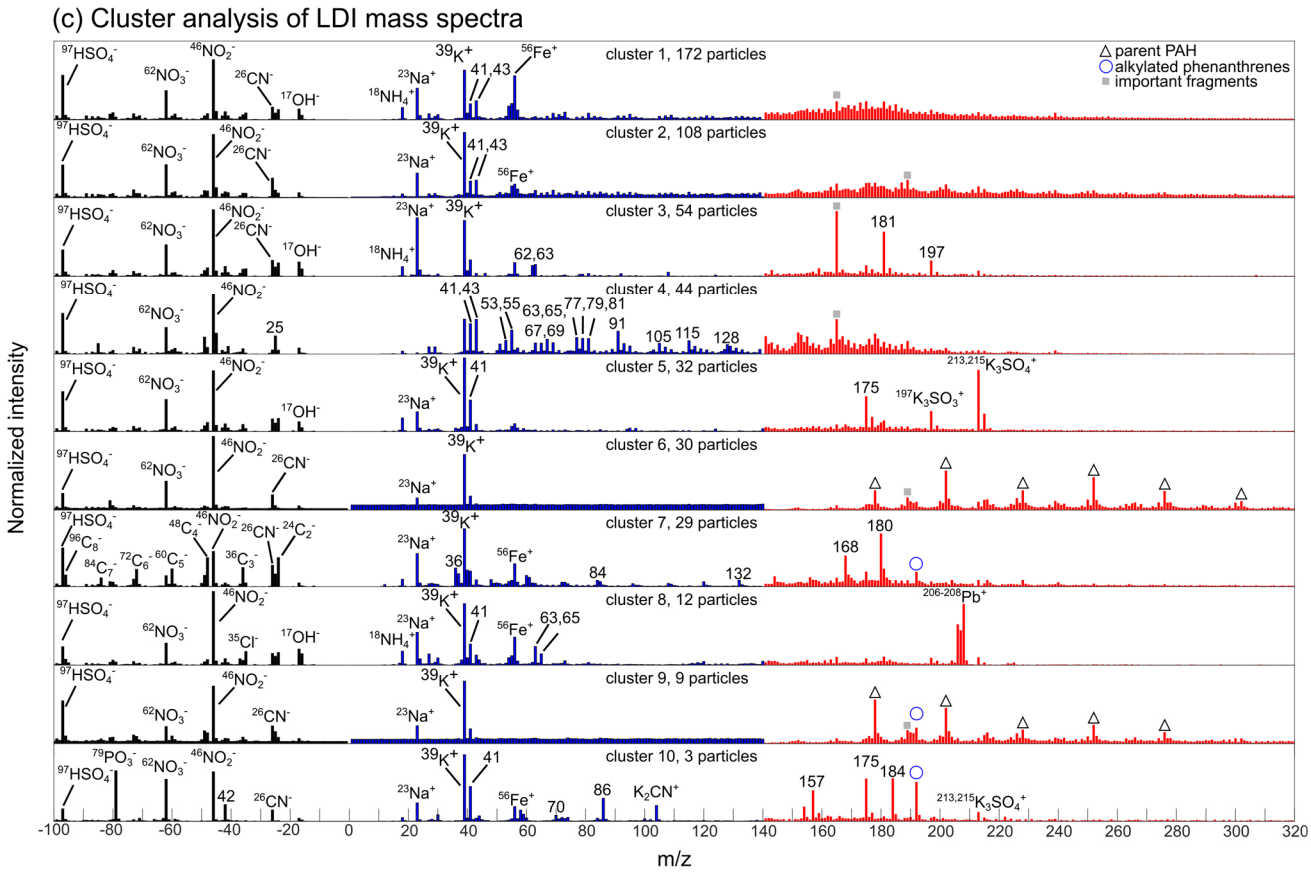

Figure S8 Results of the ART-2a cluster analyses, each including 500 PAH mass spectra from the respective ionization scheme. The combined LD-REMPI/LDI scheme yields comparable cluster centers and numbers of particles in each cluster for **(a)** using the CO2 laser and **(b)** using the Er:YAG laser for the LD step. **(c)** The single-step LDI scheme yields fewer clusters due to its higher fragmentation and lower sensitivity. The most abundant clusters are dominated by unidentified fragment signals. Only 39 out of 500 particles show clear PAH signatures for LDI.

References

Brege, M. A., China, S., Schum, S., Zelenyuk, A., and Mazzoleni, L. R.: Extreme Molecular Complexity Resulting in a Continuum of Carbonaceous Species in Biomass Burning Tar Balls from Wildfire Smoke, ACS Earth Space Chem., 5, 2729–2739, https://doi.org/10.1021/acsearthspacechem.1c00141, 2021.

Dall'Osto, M., Beddows, D. C. S., McGillicuddy, E. J., Esser-Gietl, J. K., Harrison, R. M., and Wenger, J. C.: On the simultaneous deployment of two single-particle mass spectrometers at an urban background and a roadside site during SAPUSS, Atmos. Chem. Phys., 16, 9693–9710, https://doi.org/10.5194/acp-16-9693-2016, 2016.

Healy, R. M., Evans, G. J., Murphy, M., Sierau, B., Arndt, J., McGillicuddy, E., O'Connor, I. P., Sodeau, J. R., and Wenger, J. C.: Single-particle speciation of alkylamines in ambient aerosol at five European sites, Analytical and bioanalytical chemistry, 407, 5899–5909, https://doi.org/10.1007/s00216-014-8092-1, 2015.

Jacobson, M. Z.: Investigating cloud absorption effects: Global absorption properties of black carbon, tar balls, and soil dust in clouds and aerosols, J. Geophys. Res., 117, https://doi.org/10.1029/2011JD017218, 2012.

Li, C., He, Q., Schade, J., Passig, J., Zimmermann, R., Meidan, D., Laskin, A., and Rudich, Y.: Dynamic changes in optical and chemical properties of tar ball aerosols by atmospheric photochemical aging, Atmos. Chem. Phys., 19, 139–163, https://doi.org/10.5194/acp-19-139-2019, 2019.